SATELLITE PIGMENT RETRIEVALS FOR OPTICALLY SHALLOW WATER

Kendall L. Carder, Zhong Ping Lee and F. Robert Chen
University of South Florida, 140 7 Ave. S., St. Petersburg, FL 33701, USA

INTRODUCTION

The inner continental shelves of the world ocean play important roles in terms of transitioning riverine water, carbon, and nutrients to the ocean. This region provides cover for larval fish and other larvae as well as food for grazers, with major phytoplankton blooms typically found at the mouths of estuaries. The inner shelf supports primary production by phytoplankton, macrophytes, benthic micro-flora [e.g. benthic diatoms], and by recycling nutrients through the benthic community, providing annually up to 2800 g C m^{-2} for kelp forests and from 120 to 1000 g C m^{-2} for other macrophytes [Lalli and Parsons 1993], and as much as 892 g C m^{-2} by benthic microflora [Grontved 1962]. In fact for oligotrophic shelves, there are usually higher areal chlorophyll concentrations and primary productivity in the sediments than found in the overlying water column, sometimes by as much as 4 to 6 fold [Cahoon and Cooke 1992].

In order to retrieve the bottom depth, the water-column contributions and optical properties of the water column must be known or derived. Similarly, to retrieve water-column properties, the bottom contribution must be known or derived. Historically, values for water-column contributions were approximated from values of adjacent deep waters [e.g., Polcyn et al. 1970; Lyzenga 1978, O'Neill et al. 1989], and light-attenuation values were assumed known *a priori* [e.g., Polcyn et al. 1970, Paredes and Spero 1983], or they were empirically derived from an image by regression using a few known depths provided by LIDAR or on-site ship measurements [Lyzenga 1985, Philpot 1989]. All of these methods require knowledge of a few actual depths or accurate attenuation values.

To be able to derive properties of shallow-water environments routinely, it is desired to ***simultaneously*** derive bottom depth and albedo and the optical properties of the water column. The model-driven optimization technique developed by Lee et al. [1999] demonstrated that most of the underwater information could be derived from hyperspectral, measured remote-sensing reflectance, and Lee et al. [submitted] have derived accurate bathymetry and water-column properties for turbid Tampa Bay ($1<c<2.5$ m^{-1}) using Airborne Visible Infra-Red Imaging Spectroradiometer (AVIRIS) data. AVIRIS data has 20-m pixels and 10-nm spectral resolution from 400 to 2400 nm, appropriate for bays and estuaries, but not for repeatedly examining large areas such as the west Florida shelf. By binning pixels and spectral channels, however, AVIRIS data provides a means of simulating the performance of several different sensors.

INVERTING REMOTE-SENSING REFLECTANCE (R_{RS})

Remote-sensing reflectance (R_{rs}) is an apparent optical property [Preisendorfer 1976], controlled by the absorption coefficient, scattering properties, and the bottom albedo and depth. It is also influenced by fluorescence and Raman emission [Marshall and Smith 1990, Lee et al. 1994] and by the angles of solar input and output radiance [Morel and Gentili 1993]. For waters with vertical homogeneity, and ignoring the inelastic scattering contributions,

$$R_{rs}(\lambda) = f[a(\lambda),\ b_b(\lambda),\ \rho(\lambda),\ H,\ \theta_w,\ \theta_v,\ \varphi], \quad (1)$$

where $a(\lambda)$ is the absorption coefficient, $b_b(\lambda)$ is the backscattering coefficient, $\rho(\lambda)$ is the bottom albedo, H is the bottom depth, θ_w is the sub-surface solar zenith angle, θ_v is the sub-surface viewing angle from nadir, and φ is the viewing azimuth angle from the solar plane.

To be able to routinely derive properties of shallow-water environments, it is desired to ***simultaneously*** derive bottom depth and albedo and the optical properties of the water column. The model-driven optimization technique developed by Lee et al. [1999] demonstrated that most of the under-water information could be derived from the measured remote-sensing reflectance.

Briefly recalling from [Lee et al. 1999; submitted], for $\varphi = 90^o$, the semi-analytical model (SA-model) for R_{rs} is

$$R_{rs} \approx \frac{0.5\, r_{rs}}{1 - 1.5\, r_{rs}},$$

$$r_{rs} \approx r_{rs}^{dp}\left[1 - \exp\left(-\left(\frac{1}{\cos(\theta_w)} + \frac{D_u^C}{\cos(\theta_v)}\right)\kappa H\right)\right] + \quad (2)$$

$$\frac{1}{\pi}\rho \exp\left(-\left(\frac{1}{\cos(\theta_w)} + \frac{D_u^B}{\cos(\theta_v)}\right)\kappa H\right),$$

and

$$r_{rs}^{dp} \approx (0.084 + 0.170u)u. \quad (3)$$

r_{rs} is the sub-surface remote-sensing reflectance, or ratio of the upwelling radiance to downwelling irradiance evaluated just below the surface, and $r^{dp}{}_{rs}$ is the remote-sensing reflectance for optically deep waters.

The first term on the right side of the r_{rs} equation expresses the truncation of the path radiance expected for non-reflecting bottom at depth H, while the second term expresses the actual bottom contribution at the surface after attenuated by the two-way path through the water column. In q.2, there are two optical path-elongation factors: one for photons from the water column ($D^C{}_u$), and the other for photons from bottom ($D^B{}_u$). These are approximated as [Lee et al. 1999]

$$D^C{}_u \approx 1.03(1+2.4u)^{0.5}, \text{ and } D^B{}_u \approx 1.04(1+5.4u)^{0.5}. \quad (4)$$

u and κ in Eqs.2-4 are defined as,

$$u = b_b/(a+b_b),\ \kappa = a+b_b, \quad (5)$$

$$b_b = b_{bw} + b_{bp}, \quad (6)$$

and,

$$a = a_w + a_\phi + a_g. \quad (7)$$

Note that both u and κ are inherent optical properties, and it is the combination of Eqs.2-7 that provides the expression for R_{rs}. In Eq.2, 0.5/(1-1.5 r_{rs}) is the water-to-air divergence factor [Gordon et al. 1988, Mobley 1994], and (1-1.5 r_{rs}) accounts for the internal reflection of the water-air interface, which is important when r_{rs} values get high for very shallow and/or very turbid waters. b_{bw} is the backscattering coefficient of pure seawater, b_{bp} is the backscattering coefficient of suspended particles, a_ϕ is the absorption coefficient for phytoplankton pigments, and a_g is the absorption coefficient for gelbstoff and detritus [Carder et al. 1991].

$a_\phi(\lambda)$ is simulated by a single-parameter model [Lee et al. 1998]:

$$a_\phi(\lambda) = [a_0(\lambda) + a_1(\lambda)\ln(P)]\,P, \quad (8)$$

with $P = a_\phi(440)$, the variable for phytoplankton absorption coefficient at 440nm. This approach allows $a_\phi(\lambda)$ curvature to change with $a_\phi(440)$ value, consistent with field observations, at least to first order. Values for $a_0(\lambda)$ and $a_1(\lambda)$ are provided in Table 1.

$a_g(\lambda)$ is expressed as [Bricaud et al. 1981, Carder et al. 1989]

$$a_g(\lambda) = G\, e^{-S(\lambda-440)}, \quad (9)$$

with $G = a_g(440)$. S is the spectral slope, and a value of 0.015nm^{-1} is used as a representative average in our inversion process. This S value as well as $a_0(\lambda)$ and $a_1(\lambda)$ values can be replaced if site-specific knowledge is available.

$b_{bp}(\lambda)$ is expressed as

$$b_{bp}(\lambda) = X\left(\frac{400}{\lambda}\right)^Y, \quad (10)$$

where $X = b_{bp}(400)$, which explicitly combines the particle backscattering coefficient, view-angle information as well as sea state into one variable [Lee et al. 1999]. Y is the spectral shape parameter of particle backscattering. A value of 0.5 is used for all the pixels of this study, consistent with more turbid waters [Lee et al. 1999].

$\rho(\lambda)$ is expressed using 550 nm-normalized, sand- or grass-albedo shapes, i.e.,

$$\rho(\lambda) = B\,\rho_{sand}(\lambda)\ , \text{ or } \rho(\lambda) = B\,\rho_{grass}(\lambda), \quad (11)$$

where B is the bottom albedo value at 550nm. $\rho_{sand}(\lambda)$ and $\rho_{grass}(\lambda)$ were from earlier field measurements [Lee et al., unpublished data, 1992]. We used the following empirical criteria to initially separate sand from grass bottoms: if $R_{rs}(\lambda)$ of a pixel satisfies

$$R_{rs}(550) < 0.01 \text{ and } R_{rs}(710)/R_{rs}(670) > 1.2,$$

spectral shape of ρ_{grass} is used; otherwise, spectral shape of ρ_{sand} is used.

After the above empirical/semi-analytical models are assembled,

$$\begin{aligned} R_{rs}(\lambda_1) &= F(a_w(\lambda_1), b_{bw}(\lambda_1), \boldsymbol{P, G, X, B, H}) \\ R_{rs}(\lambda_2) &= F(a_w(\lambda_2), b_{bw}(\lambda_2), \boldsymbol{P, G, X, B, H}) \\ &\vdots \\ R_{rs}(\lambda_n) &= F(a_w(\lambda_n), b_{bw}(\lambda_n), \boldsymbol{P, G, X, B, H}) \end{aligned} \quad . \quad (12)$$

There are only 5 variables required to solve Eq.12: *P, G, X, B,* and *H*. These 5 variables uniquely influence the $R_{rs}(\lambda)$ spectrum. Over-determining this equation using at least 7 spectral channels, avoids the possibility of a singularity arising.

An optimization type of model-inversion scheme is used which adjusts the values of *P, G, X, B* and *H* in Eq.13 to minimize a predefined *err* function [Lee et al. 1999; submitted]:

$$err = \frac{\left[\sum_{400}^{675}\left(R_{rs} - \hat{R}_{rs}\right)^2 + \sum_{750}^{800}\left(R_{rs} - \hat{R}_{rs}\right)^2\right]^{0.5}}{\sum_{400}^{675} R_{rs} + \sum_{750}^{800} R_{rs}}, \quad (13)$$

using predicted $\hat{R}_{rs}$ values from Eq.12 and measured R_{rs} values from AVIRIS. The cutoff between 675 and 750nm is due to the fact that no term is included in the model to express the solar-stimulated chlorophyll fluorescence presented in the measured data. Also this spectral range is greatly affected by the absorption of water vapor that is quite variable.

The computer program automatically changes the values of *P, G, X, B* and *H* until *err* reaches a minimum. At that point, values for *P, G, X, B,* and *H* are then considered to be the derived values. In the process, *P, G, X, B,* and *H* are initially set at 0.2, 0.5, 0.01, 0.05 and 2.5, respectively, and are all kept positive. Note that no field data are required/used except the aircraft- or satellite-derived $R_{rs}(\lambda)$ curves. Knowledge of time- and space-dependent regional values for S, $a_0(\lambda)$ and $a_1(\lambda)$ values, however, can improve retrieval quality for a given site and season.

EMPIRICAL CHLOROPHYLL ALGORITHM

An empirical algorithm for chlorophyll-a concentration is the OC-2 formula [O'Reilly et al. 1998], which is used to simulate bottom effects on pigment retrievals.

$$[C] = 10^{0.341 - 3.001\gamma + 2.811\gamma^2 - 2.041\gamma^3} - 0.04, \qquad (14)$$

with $\gamma = \log(R_{rs}(490)/R_{rs}(555))$. While other pigment algorithms can be used, this simple 2-wavelength algorithm is useful to demonstrate the relative errors induced by the presence of a bottom typical of the WFS.

TEST IMAGERY

Two flight lines of AVIRIS imagery of the WFS were collected on 24 May 1999 from 20 km altitude to study the possibility of retrieving useful SeaWiFS and MODIS imagery of pigments and inherent optical properties (IOPs) for shallow, coastal waters. Bottom contributions are visible out to 45 km offshore. The hyperspectral, 20 m data were vicariously calibrated and atmospherically corrected [Carder et al. 1993] and inverted [Lee et al. 1999; Lee et al. submitted] to derive bottom albedo and depth, absorption and back-scattering coefficients, and pigments. The AVIRIS data were then degraded to the spectral characteristics of MODIS to evaluate how well water-column characteristics could be retrieved with only 7 wavelengths (412, 443, 490, 531, 551, 645, 667 nm). The infrared channels were assumed to be unavailable for use since they are used in MODIS processing to correct for atmospheric effects. A histogram of the $R_{rs}(550)$ scene before bottom-correction is shown in Figure 1a for the scene in Plate 1, which had depths from 12 to 20 m.

The water-column and bottom contributions to $R_{rs}(\lambda)$ were separated for MODIS-simulated data on the WFS. The derived water-column properties were used to simulate a deep water column (i.e. the term $r^{dp}{}_{rs}$ in Eq. 2 was derived). Then Eq. 14 was applied to $r^{dp}{}_{rs}$ spectra to derive corrected chlorophyll imagery for comparison with chlorophyll images created using uncorrected data.

The corrected-chlorophyll histogram (Fig. 2a) has a bimodal distribution with a primary mode at 0.40 mg m^{-3} and a secondary mode at 0.53 mg m^{-3}. The uncorrected-chlorophyll histogram (Fig. 2b) is also somewhat bimodal, with a primary mode at 0.70 and a secondary mode at 0.60 mg m^{-3}. The bimodality of these chlorophyll histograms is not correlated to any obvious bimodality inherent in the bottom-albedo histogram (Fig. 1b), but Fig. 2a does mimic somewhat the shape of the $R_{rs}(550)$ histogram (Fig. 1a). The similarity in the secondary mode of the corrected-chlorophyll and $R_{rs}(550)$ histograms suggests that the secondary peak is probably due to incomplete removal of bright bottom effects in correcting the chlorophyll image.

Field data [W. Hou and D. Costello, unpublished] for the WFS indicate that algae-free, sandy-bottom locations (15-17% albedo at 550 nm) were brighter than hard- or gravel-bottom sites (10-12%), with darker albedos likely due to bottom cover by macrophytes and algal mats. Except near the mouths of estuaries, chlorophyll *a* concentrations for the inner WFS during the May to August period are between 0.2 and 0.5 mg m^{-3} [Carder et al. 1986; NASA SeaBASS data base].

CONCLUSIONS

AVIRIS data are used to simulate the utility of MODIS or SeaWIFS data to remove bottom effects from shallow-water imagery for the WFS collected from space. The primary-modal chlorophyll values (Fig. 2a) corrected for bottom effects using methodologies developed by Lee et al. [1999] are consistent with historical data for the region. The uncorrected values (Fig. 2b) and those under the secondary peak for the "corrected" histogram, however, are higher still by perhaps 75% and 26%, respectively. Although the secondary mode in Figure 2a is higher than the primary mode by about 26%, suggesting incomplete removal of the bottom effects over bright pixels, it still falls within the 35% accuracy objectives of the SeaWiFS Project [Hooker et al. 1992] relative to a "true" value of about 0.40 mg m^{-3}. Comparison with retrievals using hyperspectral data suggest that addition of a channel at about 610 nm would have a significant positive impact on improving the accuracy of retrievals of water-column and bottom properties for shallow waters [Lee and Carder 1999].

REFERENCES CITED

Bricaud, A., A. Morel, and L. Prieur, Absorption by dissolved organic matter of the sea (yellow substance) in the UV and visible domains, *Limnology and Oceanography*, *26* (1), 43-53, 1981.

Cahoon, L.B. and J.E. Cooke, Benthic microalgal production in Onslow Bay, North Carolina, *Marine Ecol. Prog. Series, 84,* 185-196, 1992.

Carder, K.L., S.K. Hawes, K.A. Baker, R.C. Smith, R.G. Steward, and B.G. Mitchell, Reflectance model for quantifying chlorophyll a in the presence of productivity degradation products, *Journal of Geophysical Research*, *96* (C11), 20,599-20,611, 1991.

Carder, K.L., P. Reinersman, R.F. Chen, F. Muller-Karger, C.O. Davis, and M. Hamilton, AVIRIS calibration and application in coastal oceanic environments, *Remote Sensing Environ.*, *44*, 205-216, 1993.

Carder, K.L., R.G. Steward, G.R. Harvey, and P.B. Ortner, Marine humic and fulvic acids: their effects on remote sensing of ocean chlorophyll, *Limnology and Oceanography*, *34* (1), 68-81, 1989.

Carder, K.L., R.G. Steward, J.H. Paul, and G.A. Vargo, Relationships between chlorophyll and ocean color constituents as they affect remote-sensing reflectance models, *Limnology and Oceanography*, *31* (2), 403-413, 1986.

Gordon, H.R., O.B. Brown, R.H. Evans, J.W. Brown, R.C. Smith, K.S. Baker, and D.K. Clark, A semianalytical radiance model of ocean color, *Journal of Geophysical Research*, *93* (D9), 10,909-10,924, 1988.

Grotved, J., Preliminary report on productivity of microbenthos and phytoplankton in the Danish Wadden Sea, *Meddr. Danm. Fisk.-og Havunders, 3,* 347-378, 1962.

Hooker, S.B., W.E. Esaias, G.C. Feldman, W.W. Gregg, and C.R. McClain, An overview of SeaWiFS and Ocean Color, pp. 24pp, NASA, Greenbelt, MD, 1992.

Lalli, C.M., T.R. Parsons, *Biological Oceanography: An Introduction*, Pergamon Press, 301 pp, 1993.

Lee, Z.P., K.L. Carder, Model for the interpretation of hyperspectral remote-sensing reflectance, *Applied Optics*, *33* (24), 5721-5732, 1994.

Lee, Z.P., K.L. Carder, Spectral channels and their influence on remote-sensing retrievals: 1. Shallow waters, *EOS, Trans. Amer. Geophys. U., 80(49),* p275, 1999.

Lee, Z.P., K.L. Carder, C.D. Mobley, R.G. Steward, and J.S. Patch, Hyperspectral remote sensing for shallow waters. 1. A semianalytical model, *Applied Optics*, *37* (27), 6329-6228, 1998.

Lee, Z.P., K.L. Carder, C.D. Mobley, R.G. Steward, and J.S. Patch, Hyperspectral remote sensing for shallow waters: 2. Deriving bottom depths and water properties by optimization., *Applied Optics*, *38* (18), 3831-3843, 1999.

Lee, Z. P., Kendall. L. Carder, F. Robert Chen and Thomas G. Peacock, Properties of the water column and bottom derived from AVIRIS data, *submitted, JGR*, 2000.

Lyzenga, D. R., Passive remote-sensing techniques for mapping water depth and bottom features, *Appl. Opt. 17*, 379-83, 1978.

Lyzenga, D. R., Shallow-water bathymetry using combined lidar and passive multispectral scanner data, *Int. J. Remote Sensing, 6*, 115-125, 1985.

Marshall, B. R. and R. C. Smith, Raman scattering and in-water ocean properties, *Appl. Opt., 29*, 71-84, 1990.

Mobley, C.D., *Light and Water: Radiative Transfer in Natural Waters*, 592 pp., Academic Press, San Diego, CA, 1994.

Morel, A., and B. Gentili, Diffuse reflectance of oceanic waters: II. Bidirectional aspects, *Applied Optics*, *32* (33), 6864-6879, 1993.

O'Neill, N. T. and J. R. Miller, On calibration of passive optical bathymetry through depth soundings analysis and treatment of errors resulting from the spatial variation of environmental parameters, *Int. J. Remote Sensing 10*, 1481-1501, 1989.

O'Reilly, J.E., S. Maritorena, B.G. Mitchell, D.A. Siegel, K.L. Carder, S.A. Garver, M. Kahru, and C. McClain, Ocean color chlorophyll algorithms for SeaWiFS, *Journ. Geophys. Res.*, *103* (C11), 24,937-24,953, 1998.

Philpot, W.D., and A. Vodacek, Laser-induced fluorescence: limits to the remote detection of hydrogen ion, aluminum, *Remote Sens. Environ.*, *29*, 51-65, 1989.

Paredes, J. M. and R. E. Spero, Water depth mapping from passive remote sensing data under a generalized ratio assumption, *Appl. Opt. 22*, 1134-1135, 1983.

Polcyn, F. C., W. L. Brown, and I. J. Sattinger, The measurement of water depth by remote-sensing techniques, Rep. 8973-26-F (Willow Run Laboratories, University of Michigan, Ann Arbor, Mich., 1970).

Preisendorfer, R. W., *Hydrologic optics vol. 1: introduction.* NTIS PB-259 793/8ST. National Technical Information Service, Springfield, VA, 1976.

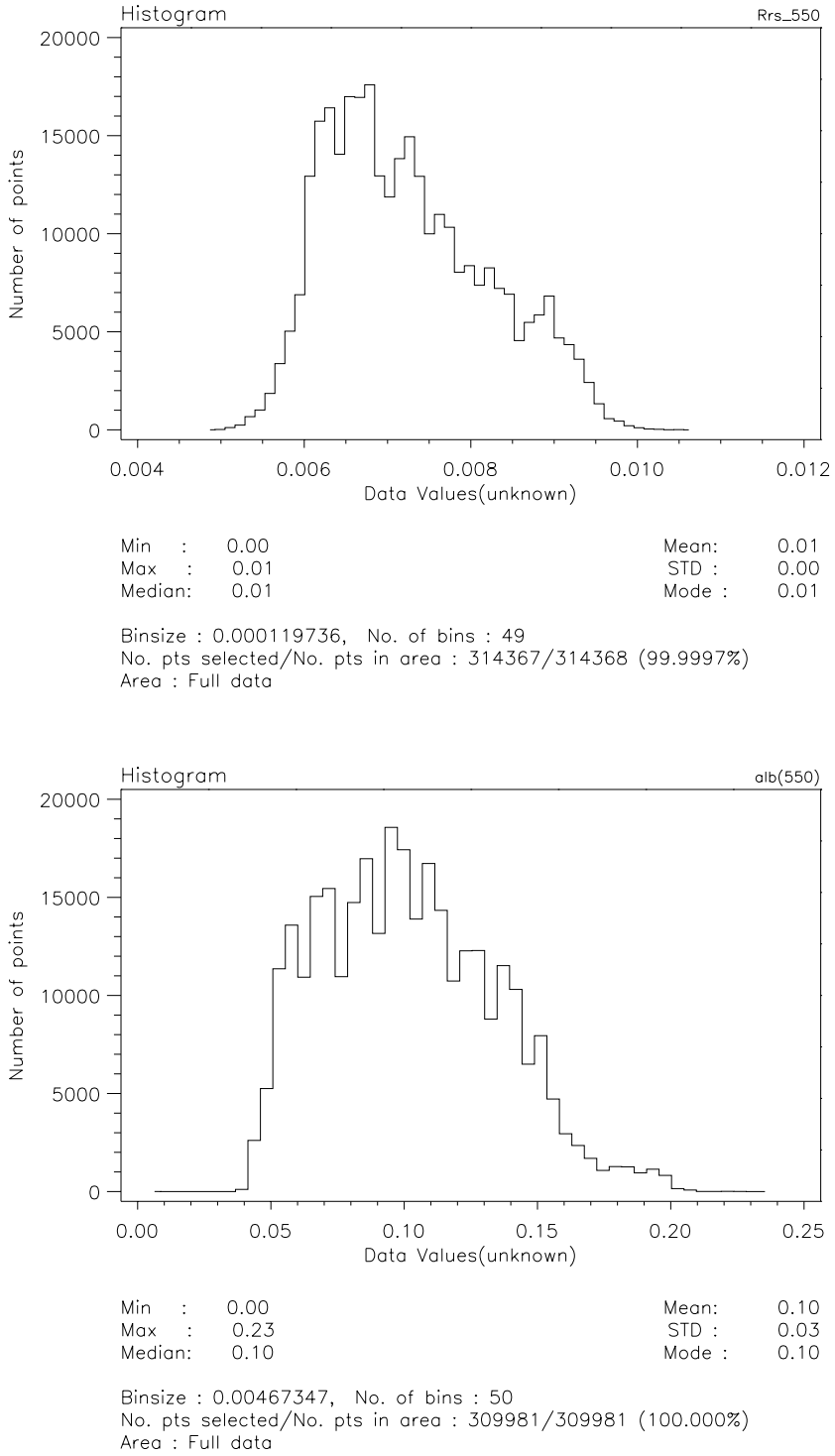

Fig. 1. Histograms of $R_{rs}(550)$ (a: upper) and bottom albedo (b: lower) for the scene in Plate 1.

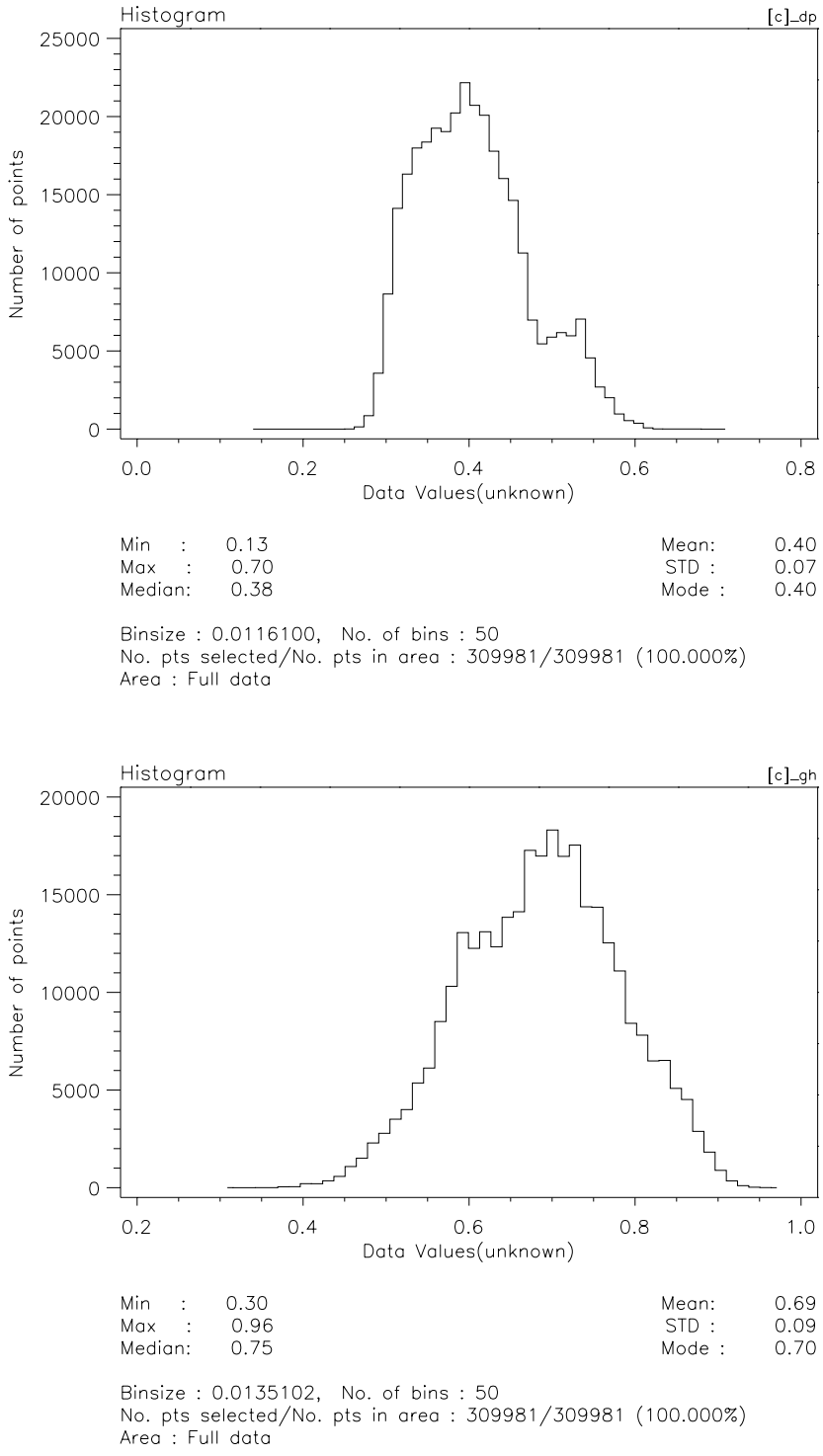

Fig. 2. Histograms of corrected (a: upper) and uncorrected (b: lower) chlorophyll-a concentrations retrieved from AVIRIS-simulated MODIS data for the image in Plate 1.

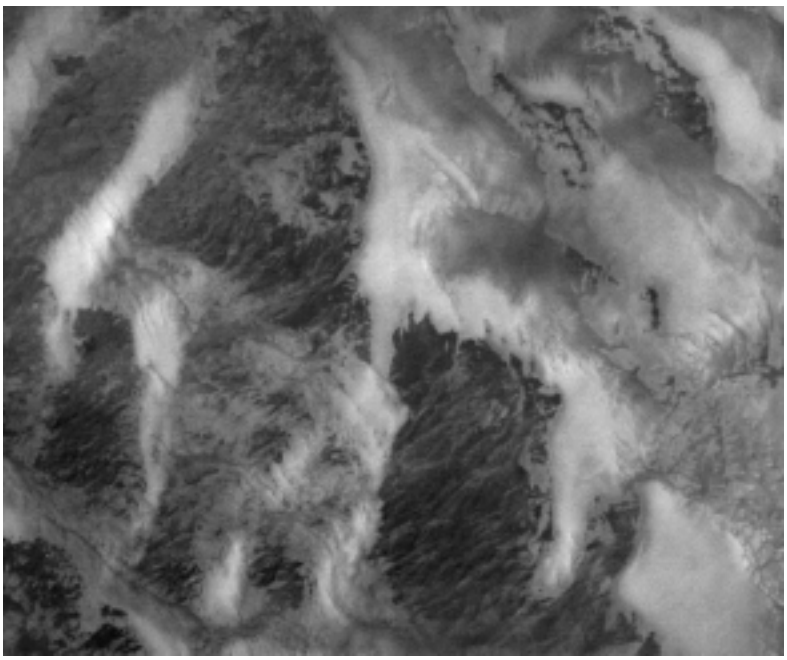

Plate 1. AVIRIS image of a scene over the West Florida Shelf some 15 to 25 km west of Egmont Key (Tampa Bay) in 12 to 20 m of water. Note the bottom features in the contrast-stretched image of radiance at 488 nm at the top of the atmosphere.